

The EasyPET: a novel concept for an educational cost-effective positron emission 2D scanner

V. Arosio, M. Caccia, I. F. Castro, P. M. M. Correia, C. Mattone, L. M. Moutinho, R. Santoro, A. L. M. Silva and J. F. C. A. Veloso

Abstract—The easyPET concept proposed here, protected under a patent by the University of Aveiro, aims to realize a simple and affordable small dimension Positron Emission Tomography (PET) scanner. This innovative system is based on a single pair of detectors and a rotating mechanism with two degrees of freedom reproducing the functionalities of an entire PET ring. A 2D imaging prototype has been designed, commissioned and engineered, targeted to high level education for physics, engineering and nuclear medicine students. In this paper the performance of the prototype is reported, with a focus on the imaging capability and on the measurement of the uncertainty in the reconstruction of the source position. In addition, a detailed analysis is dedicated to the slice sensitivity and in particular to the effect of the energy threshold on the coincidence event selection.

Index Terms—Positron Emission Tomography (PET), educational PET, small dimension PET, Silicon Photomultiplier (SiPM).

I. INTRODUCTION

POSITRON Emission Tomography (PET) is a functional medical imaging technique with a significant diagnostic power [1]. PET has a unique role in Oncology, as it allows studying the biochemical functionalities and physiologic mechanisms of organs and tissues in a non-invasive way, enabling the early identification of subtle pathologies [2]. PET is also employed to establish the stage and diffusion of a disease, to evaluate the most appropriate therapy and to monitor treatment efficacy. When combined with anatomical information through Computed Tomography (CT) or Magnetic Resonance Imaging (MRI), PET achieves a recognized superiority over other imaging modalities [3].

PET constitutes as well a key research tool for studies on small animals in preclinical research. In fact, 70-80% of small-animal PET scanners are installed in academic or government research laboratories [4]. The increasing demand for PET preclinical imaging is driven by the importance of animal model based research and by the need to conduct accurate and efficient animal experiments. PET offers the possibility to perform in vivo longitudinal studies of biochemical and molecular processes characteristic of disease onset, to monitor disease progression, evaluate therapeutic response and develop novel treatment strategies.

V. Arosio, M. Caccia and R. Santoro are with Dipartimento di Scienza e Alta Tecnologia, Università degli Studi dell'Insubria, via Valleggio 11, 22100, Como, Italy.

C. Mattone is with CAEN, via della Vetraia 11, 55049 Viareggio, Italy.

I. F. Castro, P. M. M. Correia, L. M. Moutinho, A. L. M. Silva and J. F. C. A. Veloso are with I3N, Departamento de Física, Universidade de Aveiro, Campus Universitário de Santiago, 3810-193, Aveiro, Portugal.

The need to achieve a spatial resolution at the order of one millimeter, to distinguish in small animal imaging the same level of structural detail of clinical images, and at the same time a good sensitivity represents a hard task [5]. The usually adopted solution consists in the use of scintillator crystals with a reduced cross-section facing the imaging FOV and a long side aligned with the radial direction [6], together with a method to measure the Depth Of Interaction (DOI) of the photon within the crystal. As a result, preclinical PET systems have about 20,000-30,000 scintillation crystals, with a price ranging between \$400,000-\$1,200,000, similar to that of a human PET [4]. Consequently, the high cost and complexity limit the access of academic research institutes to the PET technology.

The EasyPET is an innovative concept protected under a patent filed by University of Aveiro (WO2016147130 A1), original in its operating principle and image acquisition method, which can be exploited to achieve a simple and affordable high-performance small dimension PET system [7]. This concept is exploited to promote the knowledge of the PET technology within the student community through a user friendly, low cost, portable didactic system, using the same technology as conventional human PET scanners. The paper reports the qualification of a 2D imaging prototype with an educational purpose in terms of spatial uncertainty in the reconstruction of the source position and coincidence detection efficiency.

II. THE EASYPET CONCEPT

The easyPET concept can be introduced referring to a 2D model, where the system is designed to reconstruct the spatial distribution of a positron emitting source in a single slice. The operating principle of the proposed system is illustrated schematically in Figure 1. The educational easyPET is based on a single pair of collinear detectors and a rotating mechanism with two degrees of freedom, in order to reproduce the functionalities of an entire PET ring.

The two detectors are symmetrically mounted with respect to the centre of the FOV, which is indicated with the black dot in Figure 1. As shown in the second plot of Figure 1, the image acquisition mechanism starts with the detectors undergoing a scanning movement around an axis passing through the entrance of one of the crystals, identified with the white dot. The front face of the other crystal describes an arc of range θ along the dashed circumference centered in the scanning movement axis. In the detector position intercepting the positron source two back-to-back annihilation photons are

detected in coincidence and a Line Of Response (LOR) is identified. However, the determination of a unique azimuthal angle is not sufficient to reconstruct the (\bar{X}, \bar{Y}) coordinates indicating the source position, because a flat photon emission probability is assigned to the portion of FOV connecting the detectors.

The introduction of a second type of movement enables the source identification. In particular, the axis of the scanning movement rotates of an angle α along the solid circumference centered in the black dot, as illustrated in the third plot in Figure 1. In this new position another scan is performed and a new LOR is determined, corresponding to a different azimuthal angle.

The alternation of these two movements is repeated until a whole 360° rotation is completed. As a result, in the last plot of Figure 1 it can be seen that the crossing of the LORs obtained for the different positions of the scanning axis allows the reconstruction of the coordinates (\bar{X}, \bar{Y}) of the source, irrespective from its position inside the FOV.

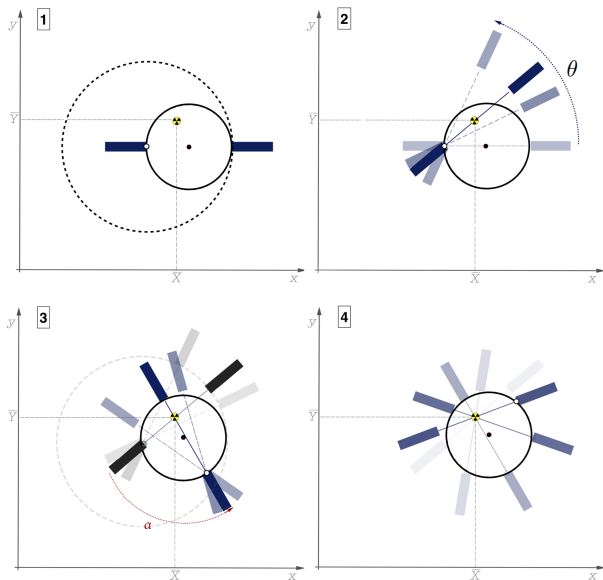


Fig. 1. The easyPET principle of operation. The detector pair executes a scan of range θ along the arc of the dashed circumference and the axis of this movement, the white dot, performs a rotation in steps of α along the solid circumference, centered in the black dot. The alternation of these two types of movement allow to determine the position of the radioactive source irrespective of its location inside the FOV.

This novel concept represents a breakthrough in terms of decreasing the system complexity and cost, by reducing the number of detectors required for the acquisition of a PET image. Moreover, thanks to the fact that the crystal pair is always kept aligned and collinear during all the data acquisition, the easyPET is intrinsically immune to parallax error and scatter radiation. In fact, the parallax error is caused by photons obliquely incident on the crystal, which penetrate neighboring crystals before being detected. This effect degrades the spatial resolution of small diameter PET systems with an uncertainty increasing with the distance of the positron source to the center of the FOV [8]. The scatter radiation is generated by the interaction of annihilation photons through Compton scattering

within the source, the environment or the scintillating crystal. The photons are deflected of a certain angle and the origin of the coincidence event is misplaced with respect to the true one. The easyPET, with a single pair of collinear crystals can not detect the obliquely incident photons nor the photons undergoing Compton scattering in neighboring crystals. As a result, a good imaging capability without aberration effects and a high spatial resolution are expected. In addition, the original implementation of the acquisition method based on two degrees of freedom ensures a uniform spatial resolution over all the FOV without the need to measure the DOI.

One potential fragility of this concept is the reduced geometrical acceptance due to the use of only two detectors, which limits the slice sensitivity of the system. The basic idea is to exploit the absence of effects degrading the image quality to partially recover the events lost because of the system geometry. In particular, the system design allows accepting also photons undergoing Compton scattering as true events, as the majority come from the photon interaction in the detecting material. Standard PET scanners have instead to discard photons below the energy of 350 keV to consider only coincidence events [9]. The easyPET approach consists in lowering the energy threshold to the level at which the random coincidence event rate is negligible in order to accept more events and enhance the overall slice sensitivity. The analysis reported in the following sections is dedicated to the measurement of the easyPET performance in order to establish the net effect of the data acquisition techniques.

III. THE 2D IMAGING PROTOTYPE

A prototype has been realized to accomplish the 2D imaging of a radioactive source through the easyPET concept and it is shown in Figure 2.



Fig. 2. The easyPET educational prototype constituted by two stepper motors, a U-shaped PCB equipped with two detecting units and a source holder.

Two stepper motors control the mechanic movement with two degrees of freedom. The bottom motor is fixed in the

FOV centre, supports and rotates the top motor, which in its turn performs the scanning. A U-shaped Printed Circuit Board (PCB), equipped with the electronic circuit and the detecting units, is attached to the axis of the top motor in correspondence of the front face of one detector. As a result, the detectors are kept aligned, placed at a distance of 5.77 cm and, depending on the range of the top motor scan, θ , are able to cover a FOV up to 50 mm.

Each detecting unit is composed by a $2 \times 2 \times 30$ mm³ LYSO scintillating crystal produced by Kinheng Crystal and coupled with an optical grease to a Silicon Photomultiplier (SiPM) of 1×1 mm² area produced by Hamamatsu Photonics (S10362-11-050P). LYSO crystals are usually employed due to their high light yield ($\sim 30,000$ photons per MeV), high density (7.18 g/cm³) and fast decay time (40 ns) [10]. SiPMs have been chosen as light detectors due to their high gain of about 10^6 , high Photon Detection Efficiency (PDE) up to 50%, compactness and low cost [11]. The specific model of SiPM used for the easyPET has a Dark Count Rate (DCR) of about 100 kHz at room temperature and a peak in the spectral response at 440 nm, matching the wavelength of the light emitted by the LYSO (420 nm). The crystal is wrapped in a white paint of BaSO₄, and then covered by an aluminum foil to optimize the light collection. The whole detecting unit is housed in a light-tight case to avoid room light to impinge directly onto the SiPMs.

The PCB integrates the detector power supplies and a fast electronic readout circuit. After a first common amplification stage of 2.5 k Ω , the output of each SiPM is divided in two branches. One branch with a single amplification stage is dedicated to spectroscopy measurements: it is required to assess the system linearity, determine the energy calibration curve and qualify the system performances in terms of light collection and energy resolution. An electronic noise at the level of 1 mV allows to distinguish the 3 mV signals corresponding to the single SiPM avalanche and perform the sensor characterization. The other branch has two additional amplification stages to saturate the signal, optimizing the coincidence counting performance, and a leading edge discriminator to select the photon energy range. Finally, an AND logic is implemented between the counting branches of the two detectors to select signals within a time gate of 120 ns, detecting the coincidence events from the same positron decay process.

The PCB integrates as well an Arduino UNO module, equipped with Adafruit motor shield and USB interfaced to a Computer to steer the two stepper motors. This microcontroller based unit is also responsible for the counting of the number of coincidences that occur at each scanning position of the detector pair. This information is then communicated to the Computer in order to accumulate the counts of each LOR and reconstruct in real-time the image of the source distribution by simply back-projecting the acquired data.

A Graphic User Interface (GUI) programmed with Visual Basic constitutes the control software which allows setting the acquisition parameters, performing the spectrum acquisition, visualizing online both the SiPM signals and the reconstruction of the activity source distribution and recording the data for the offline analysis.

IV. SPATIAL UNCERTAINTY

The PET scanner uncertainty in the reconstruction of the source position can be evaluated by the smallest distinguishable detail level of an image [12]. Figure 3 qualitatively illustrates the easyPET imaging capability. In the back-projected image two source distributions are clearly distinguishable: they are generated by two wells in a PMMA phantom filled with ¹⁸F₂FDG, with a diameter of 5 mm and 2 mm and separated by a thickness of 1 mm.

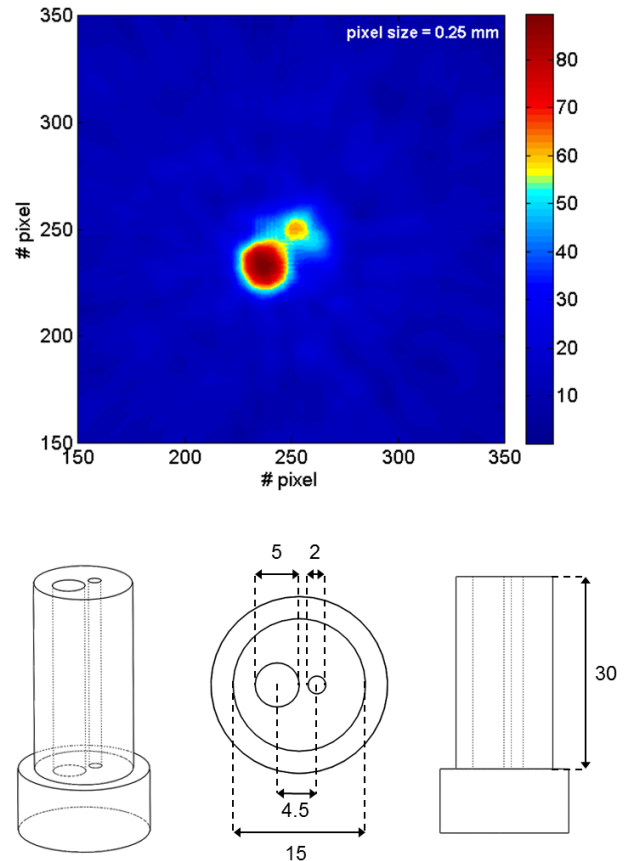


Fig. 3. The reconstructed image obtained by acquiring a total number of 6150 events in 24 minutes and the schematic layout of the phantom, with all the dimensions reported in millimeters.

An experimental setup is used to determine with a quantitative measurement the uncertainty in the reconstruction of the source position and it is sketched in Figure 4. The setup is based on the easyPET prototype: the easyPET performs a scanning movement of range θ around a 5 μ Ci ²²Na source placed in the centre of the FOV and counts the number of coincidence events at each detector pair position for 30 s.

In Figure 5 are reported the number of coincidence counts as a function of D, defined as the distance between the source and the line connecting the crystal front faces. The asymmetry in the distribution is due to the source in use: it is a radioactive solution deposited into a 3 mm deep well in a plastic disk, sealed with an epoxy [13]. When the source is positioned vertically its activity distribution results to have a sharp edge on one side, described with a Step Function, and a smoothed

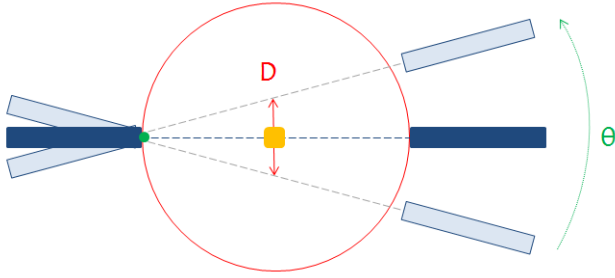


Fig. 4. The setup for the easyPET measurement of the uncertainty in the reconstruction of the source position.

edge on the other one, that is not well known. The easyPET response function is a convolution of the source activity distribution with a Gaussian function representing the spread induced by the detecting system. The lefthand side of the peak has a Gaussian behavior as it corresponds to the easyPET response function to the sharp edge activity distribution and can be exploited to measure the system uncertainty in the reconstruction of the source position [14].

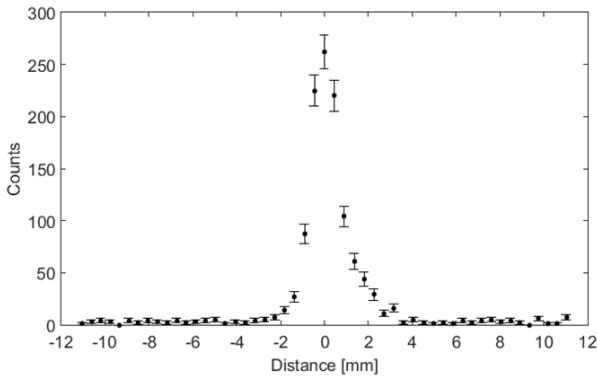


Fig. 5. The coincidence counts as a function of the distance D.

The derivative of the data points representing the measured response function is shown in Figure 6: the positive peak is related to the lefthand peak of the response function and can be fitted with a Gaussian, whose FWHM represents the system uncertainty in the reconstruction of the source position. From the fit a value of 1 ± 0.1 mm has been measured.

The easyPET uncertainty in the source position reconstruction is sufficient to distinguish the same level of structural details of human PET for rat imaging, while it is not optimal for mice imaging, where 0.4 mm FWHM is desirable [4].

As already mentioned, these imaging capability is expected to be uniform over all the FOV because, irrespective of the source position, the detection of a coincidence will occur only when the photons have a head-on interaction with the crystals. This can be demonstrated by imaging the same ^{22}Na source for the same amount of time but placed in the centre and in a peripheral region of the FOV. Figure 7 illustrates the reconstructed images and the elliptic fits applied to the data points corresponding to five times the background contribution to evaluate the reconstructed source dimensions. The ellipses

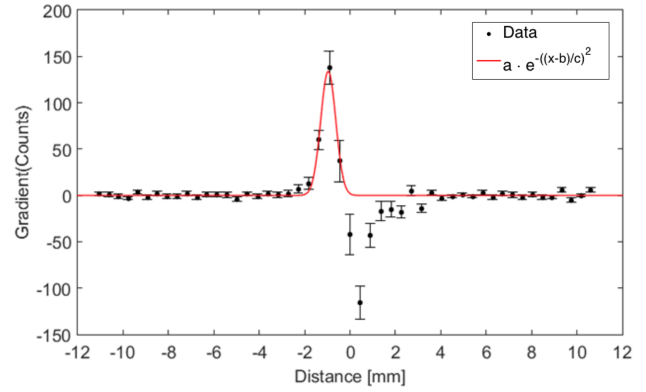


Fig. 6. The coincidence counts gradient versus D fitted with a Gaussian.

axes are compatible (6.6 mm and 7 mm for the centre and 6.8 mm and 7.2 mm for the off-centre positions), indicating that the uncertainty in the reconstruction of the source position is uniform in all the FOV.

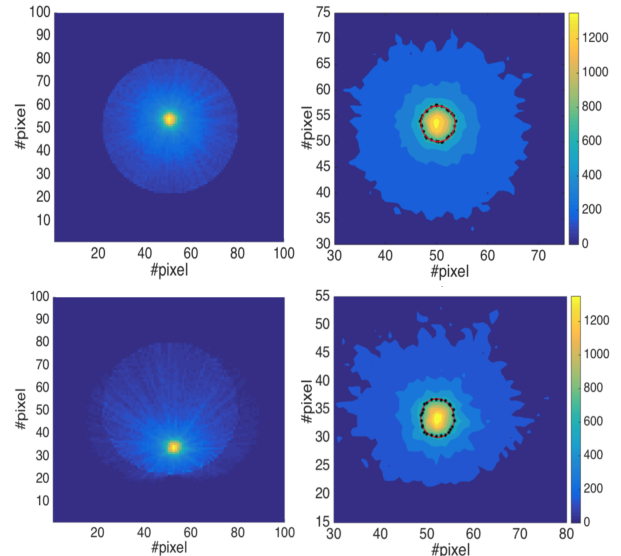


Fig. 7. The ^{22}Na source is placed in the centre (top) and in a peripheral region (bottom) of the FOV. The black stars in the zoomed plots (left) represent the contours at 5 times the background, fitted with two ellipses.

V. SLICE SENSITIVITY

The slice sensitivity can be defined as the fraction of detected positron annihilation events with respect to the total number of photons emitted back-to-back within the acceptance of the crystals. It depends both on the geometrical acceptance of the crystals and on the coincidence detection efficiency, which is the capability of the whole detecting units to reveal the photon pair impinging on the crystals. This latter quantity is a function of the scintillating material, of the photodetector features and of the electronic noise.

The system slice sensitivity represents the critical aspect of the easyPET concept, due to its reduced geometrical acceptance. A dedicated experimental setup has been designed

to study how to improve the photons detection efficiency, accounting for the alignment between the sensor and the crystal, the geometrical coupling between the sensor and the crystal and the effect of the sensor performances.

A. Experimental setup

A dedicated experimental setup, shown in Figure 8, has been realized in order to reproduce the easyPET geometry and electronic readout and allow testing various sensors under the same conditions. The mechanics has been designed to define with a reliable and reproducible procedure the alignment between the pair of sensors, of crystals and the source.

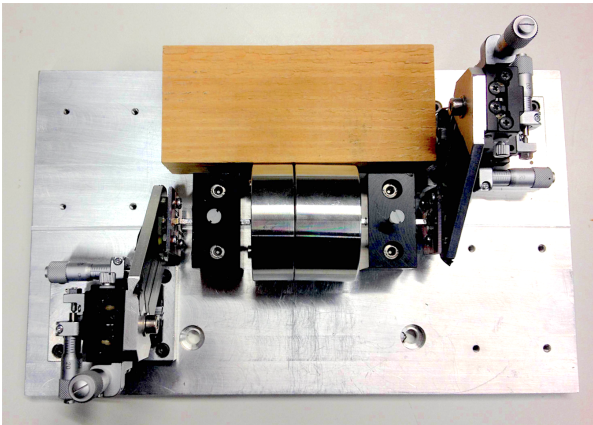


Fig. 8. The experimental setup to align, perform spectroscopy measurements and determine the coincidence detection efficiency for various SiPM areas.

The setup is composed of a metal plate on which are arranged two holders for the SiPMs, each one connected to a micro-metric handling used to adjust its position in the three spatial directions. The scintillating crystals are kept collinear through two black plastic holders drilled for all their length and fixed to the metal plate. Between the two crystals it is possible to position a collimator made out of stainless steel ($\mu = 0.66 \text{ cm}^{-1}$) and composed by two blocks with a housing in the centre for the $10 \mu\text{Ci } ^{22}\text{Na}$ radioactive source. A 1 mm diameter opening has been performed for the 4 cm length of the cylinder, in order to realize an emission hole aligned with both the scintillating crystals. As a result, the cone of coincidence photons emitted by the radioactive source is fully contained in the solid angle defined by the crystal surface, while a photon pair traveling in the collimator material has about 96% of probability to be stopped.

The crystals used are the same of the easyPET prototype, while the sensors tested are of different dimension in order to evaluate the effects of the geometrical coupling and of the sensor performance on the coincidence detection efficiency. In particular, results are reported for the easyPET prototype sensor, the $1 \times 1 \text{ mm}^2$ of Hamamatsu S10362-11-050C, and for a $2 \times 2 \text{ mm}^2$ of a new Hamamatsu generation (S13360-2050VE), perfectly matching the crystal surface [15].

The scheme of the electronic readout is the following: the SiPM output signal is split and one branch is directly fed into a Caen digitizer (DT5720A) [16] to be integrated

with a sampling rate of 250 MS/s over a 12 bit dynamic range, while the trigger is provided by the other branch, which is amplified and discriminated with a Power Supply Amplification Unit (SP5600) by Caen [16]. This electronic scheme allows performing the spectroscopy measurements and analyzing the features of the SiPM in dark conditions, which in turn permits evaluating the system response in terms of energy and of number of photons collected. At the same time, for the coincidence detection efficiency the events will be counted exploiting the trigger signals, using a counter and a coincidence logic, to reduce the rise time difference of signals of different energies and eliminate the time walk uncertainty.

The operating bias voltage at 25°C has been determined to be 73.3 V for the $1 \times 1 \text{ mm}^2$ and 55.1 V for the $2 \times 2 \text{ mm}^2$, with the correspondent gain of $8.37 \cdot 10^5 \pm 2 \cdot 10^3$ and of $1.80 \cdot 10^6 \pm 4 \cdot 10^3$. A complete characterization procedure lead to measure in this operating conditions a DCR of $(62 \pm 3) \text{ kHz}$ and $(223 \pm 3) \text{ kHz}$, an Optical Cross-Talk (OCT) of $(11 \pm 1) \%$ and $(6 \pm 0.7) \%$ and an Afterpulsing of $(16 \pm 0.6) \%$ and $(1.6 \pm 0.1) \%$ for the smaller and the bigger area sensors, respectively.

B. Crystal-SiPM alignment

The determination of the perfect alignment between the sensor and the crystal plays a crucial role and the established procedure is the following. The sensors are positioned in their holders and biased at their operating voltages, and each one is aligned independently with respect to the other, one coordinate at a time. The measurement consists in the acquisition and in the analysis of the spectra of the $10 \mu\text{Ci}$ source of ^{22}Na placed in contact with the front face of the crystal of the considered detecting unit.

The figure of merit taken into account to establish the best position is the value of the ADC channel correspondent to the 511 keV peak of the spectrum. In fact, when the sensor and the crystal are aligned, the light collected is maximized and also the integral of the signal pulse corresponds to an higher ADC channel.

In the reference system adopted the y axis is longitudinally directed as the crystal length, the x axis is perpendicular to the y and parallel to the metal plate, while the z is perpendicular to the other two axes.

As the crystals are already fixed in the correct positions, the y coordinate is determined by placing the sensor in contact with the crystal, coupled with optical grease. The x position is determined by changing the offset between the sensor and the crystal at steps of $200 \mu\text{m}$ with the micro-metric screw, acquiring the spectrum at each position, fitting the photo-peak with a Gaussian function and finding the maximum ADC value. Finally, the z is determined in the same way as x, through a scan of the sensor position perpendicularly to the metal plate. Figure 9 shows the response of the two sensors under test in terms of the variation of the photo-peak position as a function of the z of the sensor: the optimal z position of the sensors corresponds to the maximum of the curve.

This measurement can also be exploited to establish the tolerance required in the alignment between the sensor and

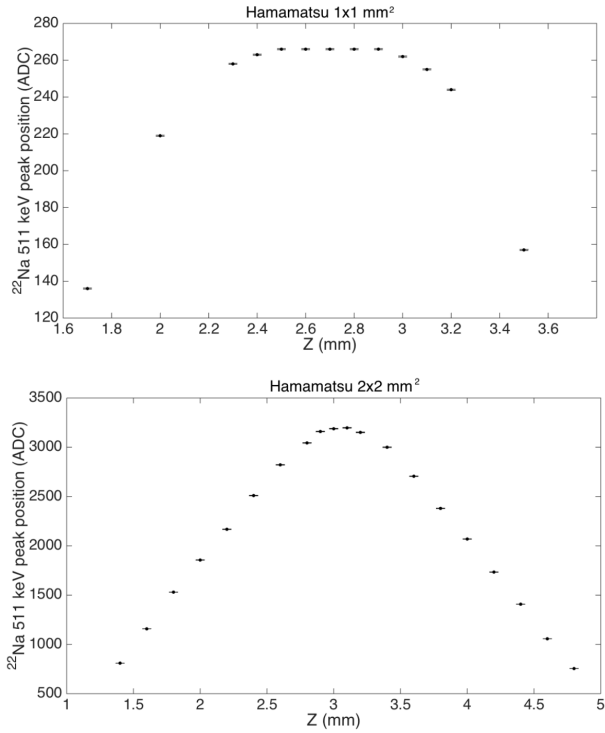


Fig. 9. The 511 keV peak in ADC as a function of the sensor position in the z direction with respect to the crystal.

the crystal. It can be inferred that for the small area sensor the alignment is not really an issue: the position of the peak has a plateau in the centre and starts to decrease significantly when the displacement between the crystal and the sensor is of 0.4 mm. Instead, it is worth to highlight that a relative misalignment of 0.4 mm will cause a 13% decrease in the peak position for the large area sensor, leading to a loss of about 110 photons (the conversion between channels and number of photons is obtained by considering the sensor peak-to-peak distance at the operating voltage and the amplification factor).

C. Crystal-SiPM geometrical coupling

After having determined the perfect alignment for the two sensors, the ^{22}Na spectra are acquired for 20 minutes with the sensors biased at their operating voltages. The spectra are obtained by integrating the split SiPM output during a gate of 200 ns for the small area sensor and 300 ns for the other one. The trigger is provided by the other branch of the SiPM output, amplified 40 times and discriminated at 25 mV for the $1\times 1\text{ mm}^2$ and at 50 mV for the $2\times 2\text{ mm}^2$; the threshold has been chosen as the minimum value that allows eliminating the SiPM noise in the low spectra region. In order to subtract the background due to the LYSO self-activity the spectra are also acquired for the same amount of time but without the radioactive source: they result to represent a very negligible contribution to the whole source spectra.

In Figure 10 are shown with solid lines the source energy spectra with the LYSO background subtracted for the two sensors: it is possible to infer that the quality of the spectrum corresponding to the $2\times 2\text{ mm}^2$ sensor is better and the detailed

structures of the backscattering peaks and the peak at 1275 keV can be clearly distinguished.

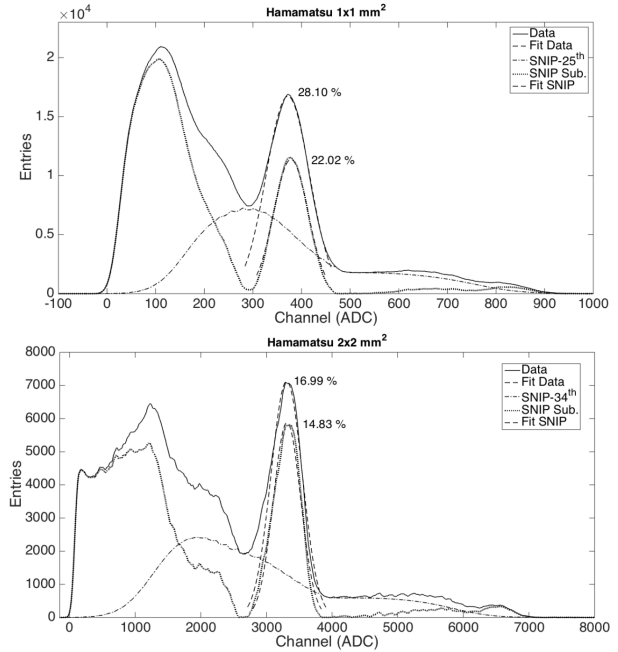


Fig. 10. The ^{22}Na spectra obtained for a SiPM of $1\times 1\text{ mm}^2$ and $2\times 2\text{ mm}^2$ with the LYSO background subtracted (solid lines), the Compton scattering contribution estimated with the SNIP algorithm (dash-dot lines) and the difference of the two is represented by the dotted distribution. The Gaussian fit to the peaks are represented by the dashed lines.

In order to determine the energy resolution of a photo-peak due only to the system resolution, it is necessary to estimate and eliminate the contribution of the underlying physics processes that are considered as a background. In fact, in order to separate the Compton events from the information of the photo-peak, the spectra are processed with the flexible and widely used method of Sensitive Nonlinear Iterative Peak (SNIP) algorithm [17],[18]. The iterative procedure is stopped when the estimated background is monotonically changing in the peak region or it drops below 5% of the total area underneath the peak. In Figure 10 are also reported with the dash-dot lines the estimated backgrounds due to the Compton scattering and with dotted lines the background subtracted spectra: the SNIP procedure is correct as the peak side wings of these latter distributions fluctuate around zero. A fit to the photo-peaks allows to determine the energy resolution at 511 keV: it results to be $(22.02\pm 0.01)\%$ for the small area sensor and $(14.83\pm 0.01)\%$ for the large area sensor. The latter values represent a fairly good result, as it is dominated by the irreducible intrinsic resolution of the LYSO.

The peak-to-total ratio have been calculated by normalizing the areas underneath the 511 keV peaks to the total areas of the correspondent spectra. The peak-to-total ratio results to be $(28.1\pm 0.1)\%$ for the $1\times 1\text{ mm}^2$ and $(25.1\pm 0.1)\%$ for the $2\times 2\text{ mm}^2$. In general, these values are in agreement with the value of 25.5% attributed to the LYSO photon fraction: it means that the fraction of the area under the photo-peak with respect to the area under the Compton continuum corresponds the ratio

between the photoelectric and the Compton cross-sections of the detector material.

The last quantity that has to be considered is the number of photons collected in the photo-peak. After the SiPM characterization, and in particular the acquisition of the spectrum in dark conditions, the distance between two peaks in the spectrum corresponding to one photon can be measured in ADC channels.

For the $1 \times 1 \text{ mm}^2$ it has been calculated that the number of fired cells for the 511 keV peak, located at 373 ± 1 ADC, is 241 ± 2 . As the SiPM has 400 cells, the saturation effect on the number of photoelectrons should be considered. The formula:

$$N_{fired} = N_{tot} \cdot \left(1 - e^{-\frac{N_{pe}}{N_{tot}}}\right), \quad (1)$$

where N_{fired} is the number of fired cell and N_{tot} the total number of SiPM cells, allows to correct the number of primary photoelectrons N_{pe} for the saturation, leading to the value of 369 ± 6 . Finally, by taking into account the impact of the $(11 \pm 1)\%$ of the OCT, the number of primary photoelectrons results to be 329 ± 10 . This value can be compared with the estimation of the number of photons incoming on the SiPM area. LYSO crystal produces about 16352 photons at 511 keV, then only $(25 \pm 5)\%$ of light is conveyed to the sensor (the typical percentage accounting for the light transmission of the crystal and the optical coupling grease [19]), a fourth can be detected due to the sensor geometrical acceptance and finally about 35% of this light is effectively detected due to the SiPM PDE. The expected number of primary photoelectrons is 356 ± 72 , which is in agreement with the measured value.

In the case of the $2 \times 2 \text{ mm}^2$ the spectrum has a peak at 3378 ± 4 ADC, which corresponds to 923 ± 4 photoelectrons. Considering that the sensor is composed by 1584 cells and has an OCT of $(6.0 \pm 0.7)\%$, the resulting number of primary photons is 1300 ± 20 . This is in a fairly good agreement with the value of 1635 ± 327 , the calculated number of photons impinging onto the SiPM from the hypothesis that the photons produced by the LYSO are scaled only for the the probability of light collection onto the sensor and for the 40% of PDE, as the area of the crystal and the sensor are perfectly matching.

From the comparison of the performances of the detecting unit equipped with the two sensors it can be concluded that SiPMs with large area allow obtaining a better energy resolution and collecting a higher number of photons at the photo-peak thanks to better geometrical coupling with the crystal area.

D. Coincidence Detection Efficiency

The most important figure of merit of the detecting unit performance consists in the coincidence detection efficiency, as it is the basic measurement of the easyPET. Considering that the detecting unit is dedicated to a 2D imaging prototype, it would not be fair to use as a normalization the activity of the source over the whole 3D sphere with the radius equal to the distance between the crystal and the system centre. The collimator will be employed to generate an emission cone and allow reducing the system to a toroidal region comprehending the two crystal front faces. The measurement of the coincidence emission hole

activity, which will be used as a normalization factor for the coincidence detection efficiency, is performed by embedding the ^{22}Na source inside the collimator and positioning two LYSO crystals of $6 \times 6 \times 30 \text{ mm}^3$ in contact with the collimator and optically coupled to two Hamamatsu SiPMs of $6 \times 6 \text{ mm}^2$ area (S13083-050CS), as shown in Figure 11. In this way, all the photon pairs emitted by the hole will interact in the crystals and will be detected. The logic output signal of the two discriminators, set at the lowest possible value, are fed into a coincidence logic to select only the events within a time window of 120 ns. The coincidence rate, after the subtraction of the background, was $(112 \pm 3) \text{ Hz}$.

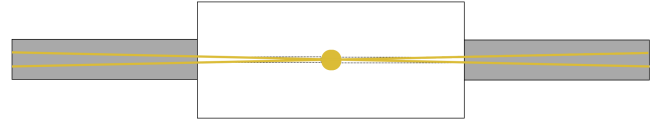


Fig. 11. A sketch of the setup used to measure the activity of the collimator emission hole: all the coincidence pairs of emitted photons are detected by the $6 \times 6 \times 30 \text{ mm}^3$ LYSO crystals coupled to the $6 \times 6 \text{ mm}^2$ Hamamatsu SiPM.

The coincidence rate measured with the $2 \times 2 \times 30 \text{ mm}^3$ LYSO crystals of the experimental setup, coupled with the two sensors under test, will lead to lower values. In fact, not all the photon pairs of the emission hole included in the solid angle of the crystals will be detected because they can not cross a sufficient quantity of scintillating material to interact ($\mu = 0.87 \text{ cm}^{-1}$), as illustrated in Figure 12. In this scenario, the coincidence rate measurement accounts also for the effective distance that a photon has to travel in order to be detected, which depends on the interaction length of the crystal material, its dimension and the energy of the photon.

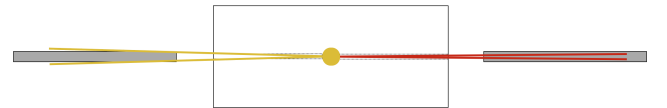


Fig. 12. The coincidence rate are measured with the $2 \times 2 \times 30 \text{ mm}^3$ LYSO crystals coupled to the sensors under test: not all the back-to-back photon pairs emitted by the hole are effectively detected due to the photon interaction probability in the LYSO.

The results of the measured coincidence detection efficiency for the two considered sensors are summarized in Table I. It can be inferred that the easyPET concept allows to lower the energy threshold, accepting more events and enhancing the coincidence detection efficiency. At each value of energy threshold, there is a slight effect related to the SiPM area: the larger the sensor area, the higher is the detection efficiency. In fact, at fixed energy, a better spectra quality ensures a better effectiveness in selecting the events above a certain threshold. The real advantage that comes from using the large area sensor is that it allows lowering even more the energy threshold and achieve a higher coincidence detection efficiency. In fact, at a fixed energy, the $2 \times 2 \text{ mm}^2$ sensor is capable to collect a huge amount of photons with respect to the small area one.

As a result, the same threshold of ten photons required to eliminate the background, corresponds to 80 keV for the 1×1 mm² SiPM and to 10 keV for the 2×2 mm². Using a sensor with area matching the cross section of the scintillating crystals it is possible to achieve a $(9.9 \pm 0.9)\%$ of coincidence detection efficiency.

TABLE I
THE COINCIDENCE DETECTION EFFICIENCY AT 350 KEV AND 150 KEV,
THE MINIMUM ENERGY THRESHOLD AND THE CORRESPONDENT
MAXIMUM COINCIDENCE DETECTION EFFICIENCY ACHIEVABLE.

SiPM	350 keV	150 keV	Min. energy	Max. efficiency
1×1 mm ²	$(0.6 \pm 0.2)\%$	$(2.9 \pm 0.6)\%$	80 keV	$(4.5 \pm 0.7)\%$
2×2 mm ²	$(1.0 \pm 0.4)\%$	$(3.3 \pm 0.5)\%$	10 keV	$(9.9 \pm 0.9)\%$

VI. CONCLUSIONS AND OUTLOOK

The easyPET concept has been presented, explaining the advantages offered by the novel data acquisition mechanism in terms of reduction of cost and complexity, which ensures an intrinsic immunity against the scatter radiation and the parallax error.

A 2D imaging prototype based on the easyPET concept has been realized and commissioned, emphasizing the good imaging capability and the ability, uniform over all the FOV, to distinguish two sources at 1 mm distance, due to the small size of the crystals, their single readout and their collinearity during all the data acquisition.

The easyPET concept has been licensed to Caen S.p.a and the prototype will become a commercial product for the educational market. The easyPET constitutes an asset in high level didactic laboratories as it opens up the possibility to teach by doing the basics of the SiPM characterization, the spectroscopy measurements together with the theoretical principles and the technology behind the PET imaging modality with a unique, user-friendly and portable device.

A dedicated setup has been designed to focus on the possible improvements to the easyPET coincidence detection efficiency, which is quite low due to the reduced geometrical acceptance. In particular, it has been demonstrated that the use of a SiPM with an area matching the crystal surface, a 2×2 mm² Hamamatsu, can optimize the quality of the spectra in terms of energy resolution and number of collected photons. As a result, the use of this sensor allows to lower the energy threshold down to 10 keV, reaching a coincidence detection efficiency of $(9.9 \pm 0.9)\%$. The studies dedicated to the investigation of the importance of the sensor-crystal alignment show that with the large area sensor a 0.4 mm displacement from the optimal position causes a loss of 13% of the collected light.

A further enhancement of the coincidence detection efficiency will be expected from an optimization of the crystals aspect ratio and coating material.

In terms of geometry, the use of multiple pairs of detectors, keeping the readout of single sensor pairs, is considered a promising solution to improve the solid angle coverage and to implement the 3D imaging functionality with performances at a level comparable to available preclinical PET systems, but without compromising the system simplicity. Ongoing

studies are devoted to the realization of a 3D easyPET imaging demonstrator.

ACKNOWLEDGMENTS

This work was partially supported by project POCI-01-0145-FEDER-016855 and PTDC/BBB-IM6/4909/2014, project easyPET n^o17823, UID/CTM/50025/2013, through COMPETE, FEDER, POCI and FCT (Lisbon) programs.

P. M. M. Correia and A. L. M. Silva are grateful to FCT (Lisbon) for scholarship BD/52330/2013 and post-doc grant SRFH/BPD/109744/2015, respectively.

The authors wish to thank Nuclear Instruments and RI-TE, for the PCB design and the assembly of the scintillation detectors for the CAEN prototypes, respectively.

REFERENCES

- [1] G. Tarantola, F.Zito, P.Gerundini, *PET instrumentation and reconstruction algorithms in whole-body applications*, J. Nucl. Med.44, 2003, 756-769.
- [2] M.E. Juweid, B.D. Cheson, *Positron-emission tomography and assessment of cancer therapy*, N. Engl. J. Med. 2006, vol. 354, 496-507.
- [3] G.K. Von Schulthess, H.C. Steinert, T.F. Hany, *Integrated PET/CT: current applications and future directions*, Radiology, 2006, vol. 238, 405-422.
- [4] R. Yao, R. Lecomte, E. S. Crawford, *Small-Animal PET: what is it, and why do we need it?*, Journal of Nuclear Medicine Technology, 2012, 40:157-165.
- [5] C. Kuntner, D. Stout, *Quantitative preclinical PET imaging: opportunities and challenges*, Frontiers in physics, 2014.
- [6] M. Larobina, A. Brunetti, M. Salvatore, *Small animal PET: a review of commercially available imaging systems*, Curr. Med. Imaging Rev. 2, 2006, 187-192.
- [7] V. Arosio, M. Caccia, I.F. Castro, P.M.M. Correia, C. Mattone, L.M. Moutinho, R. Santoro, A.L.M. Silva, J.F.C.A. Veloso, *easyPET: a novel concept for an affordable tomographic system*, Nuclear Instruments and Methods in Physics Research A, 2016, <http://dx.doi.org/10.1016/j.nima.2016.05.004i>
- [8] J.S. Lee, *emphTechnical advances in current PET and hybrid imaging systems*, The Open Nuclear Medicine Journal, 2010, 2:192-208.
- [9] A.L. Goertzen et al., *NEMA NU 4-2008 Comparison of preclinical PET imaging systems*, The Journal of Nuclear Medicine, 2012, 53:1300-1309.
- [10] A.F. Martins, J.F.C. Carreira, J. Rodrigues, N. Ben Sedrine, I.F.C. Castro, P.M.M. Correia, J.F.C.A. Veloso, L. Rino, T. Monteiro, *Spectroscopic analysis of LYSO:Ce crystals*, Spectrochimica Acta Part A: Molecular and Biomolecular Spectroscopy, Volume 172, 5 February 2017, Pages 163-167, ISSN 1386-1425, <http://dx.doi.org/10.1016/j.saa.2016.04.019>.
- [11] http://www.phys.hawaii.edu/~idlab/taskAndSchedule/iTOP/SciFi_doco/s10362-11series_kapd1022e05.pdf
- [12] G.B. Saha, *Basics of PET Imaging*, Springer, New York, 2010.
- [13] www.spectrumtechniques.com/radioisotopes.htm
- [14] B.H. Hasegawa, *The Physics of Medical X-ray Imaging*, Medical Physics Pub. Corp., 2nd edition, 1987, Chapter 6.
- [15] <http://www.hamamatsu.com/us/en/product/category/3100/4004/4113/S13360-2050VE/index.html>
- [16] <http://www.caen.it/jsp/Template2/CaenProd.jsp?parent=61&idmod=1023>
- [17] C. G. Ryan, et al., *SNIP, a statistics-sensitive background treatment for the quantitative analysis of PIXE spectra in geoscience applications*, Nuclear Instruments and Methods in Physics Research Section B, 1998, Volume 34, Issue 3, 396-402.
- [18] M. Caccia, A. Ebolese, M. Maspero, R. Santoro, *Background removal procedure based on the SNIP algorithm for X-ray spectroscopy with the CAEN Educational Kit*.
- [19] A.N. Otte, J. Barral, B. Dolgoshein, *A test of silicon photomultipliers as readout for PET*, Nuclear Instruments and Methods in Physics Research A, 2005, 545:705-715.